Naval Research Laboratory

Washington, DC 20375-5000

The Interaction of a Shock With a Compressible Vortex

JANET L. ELLZEY, MICHAEL PICONE AND ELAINE S. ORAN

Senior Science for Reactive Flow Physics Branch
Laboratory for Computational Physics and Fluid Dynamics

January 2, 1992

DTIC
ELECTE
JAN 16 1992
S B D

92-01210

REPORT DOCUMENTATION PAGE

Public reporting burden for this collection of information is estimated to average 1 hour per response, including the time for reviewing instructions, searching existing data sources, gathering and maintaining the data needed, and completing and reviewing the collection of information. Send comments regarding this burden estimate or any other aspect of this collection of information, including suggestions for reducing this burden, to Washington Headquarters Services, Directorate for Information Operations and Reports, 1215 Jefferson Davis Highway, Suite 1204, Arlington, VA 22202-4302, and to the Office of Management and Budget, Paperwork Reduction Project (0704-0188), Washington, DC 20503.

1. AGENCY USE ONLY (Leave blank)	2. REPORT DATE 1992 January 2	3. REPORT TYPE AND DATES COVERED Interim

4. TITLE AND SUBTITLE The Interaction of a Shock With a Compressible Vortex	5. FUNDING NUMBERS PE — DARPA PR — DARPA TA — 6.1 WU — 6.1
6. AUTHOR(S) Janet L. Ellzey, J. Michael Picone, and Elaine S. Oran	

7. PERFORMING ORGANIZATION NAME(S) AND ADDRESS(ES) Naval Research Laboratory Washington, DC 20375-5000	8. PERFORMING ORGANIZATION REPORT NUMBER NRL Memorandum Report 6919

9. SPONSORING/MONITORING AGENCY NAME(S) AND ADDRESS(ES) Defense Advanced Research Project Agency (DARPA) 1400 Wilson Blvd Arlington, VA 22209-2308	10. SPONSORING/MONITORING AGENCY REPORT NUMBER

11. SUPPLEMENTARY NOTES

12a. DISTRIBUTION/AVAILABILITY STATEMENT Approved for public release; distribution unlimited.	12b. DISTRIBUTION CODE

13. ABSTRACT (Maximum 200 words)

Numerical simulation of the interaction of a shock with either a single vortex or a vortex pair are used to investigate the resulting shock structure, production of acoustic waves, vortex distortion, and vorticity amplification. The study includes the interaction of strong (M=1.5) and weak (M=1.5) shocks with both strong and weak vortices which have peak velocities equal to the velocity of the fluid behind the strong and weak shocks, respectively. The simulations show that at early times, the distortion of a shock by a strong vortex can be predicted using a simple linear model. In addition, a quadrupolar wave propagates upstream as predicted by linearized theories. At later times, the interaction of the diffracted and refracted portions of the shock produces connected reflected shock structures. For the strong shock, the reflected shock structure merges with the quadrupolar wave to produce the asymmetric acoustic wave observed in experiment.

14. SUBJECT TERMS			15. NUMBER OF PAGES 38
			16. PRICE CODE

17. SECURITY CLASSIFICATION OF REPORT UNCLASSIFIED	18. SECURITY CLASSIFICATION OF THIS PAGE UNCLASSIFIED	19. SECURITY CLASSIFICATION OF ABSTRACT UNCLASSIFIED	20. LIMITATION OF ABSTRACT UL

CONTENTS

THE INTERACTION OF A SHOCK WITH
A COMPRESSIBLE VORTEX

Introduction

The interaction of a shock wave with a vortex has been the subject of active experimental study for several decades (1-10). Most of the work was motivated by an interest in the noise produced by rockets and high-speed aircraft, and therefore the research emphasized the generation of acoustic waves. For these problems, the interaction of shocks with turbulent flows is a significant source of noise (9,10). The shock-vortex system is an important element of these more complex processes. Early shock tube experiments of Hollingsworth and Richards (1) showed that the shock-vortex interaction produced a cylindrical acoustic wave, with a portion cut off by intersection of the acoustic wave with the transmitted shock. The circular portion consisted of alternating rarefactions and compressions (two each) around the circumference of the wave. The strengths of the rarefactions and compressions were different, and the compression adjoining the shock was particularly intense. Later experiments by Dosanjh and Weeks (2) measured the distribution of pressure around the circumference of the acoustic wave and found that the pattern of compressions and rarefactions was approximately quadrupolar. The compressions, however, were stronger than the corresponding rarefactions. Consistent with Hollingsworth and Richards, the strongest portion of the acoustic wave was the compression adjoining the transmitted shock.

More recent experiments by Naumann and Hermanns (3) revealed curved, diffracted shocks on either side of the vortex. The vortex flow field accelerated one of the diffracted shocks relative to the other, so that their eventual intersection produced a transmitted shock which was distorted from the initially planar shape. The intersecting shocks included additional structure beyond the merged, transmitted shock; in fact, for a strong shock interacting with a strong vortex, connected Mach structures were clearly visible. The accelerated component of this complex shock system formed an acoustic wave which propagated to the side and rear of the vortex. The acoustic wave was compressive and appeared to form only the arc of a circle.

The theories of Hollingsworth and Richards (4), Ribner (5,6), Weeks and Dosanjh (7), and Ting (8) were linear in their representations of the influence of the vortex flow field and the shock. Hollingsworth and Richards (4) applied early work by Ribner (5), who

1

decomposed a "weak" spatial distribution of vorticity into plane sinusoidal shear waves through the use of Fourier transforms. The solution of Ribner for the case of a single vortex (6) gave an acoustic wave which was perfectly quadrupolar, in that the stronger compression and rarefaction and the weaker compression and rarefaction had the same respective strengths. The theory of Weeks and Dosanjh (7) developed a representation of the acoustic wave as a sum of monopole, dipole, and quadrupole acoustic sources. The resulting fit of this equation to their experimental data was a significant improvement because it accurately represented the asymmetric pressure distribution. In his recent paper, Ribner (10) developed a physical picture which supported the theory of Weeks and Dosanjh. Ting (8) used the linearized equations of compressible flow to solve for acoustic wave production by a point vortex and then showed how to use these results to construct solutions for finite vorticity distributions. This produced a quadrupolar pressure distribution similar to that of Ribner. All of the above theories were linear, so that the distortion of the shock was assumed to be small or negligible. The experiments of Naumann and Hermanns (3) demonstrated that significant nonlinear effects are present in the form of diffracted shocks and obliquely intersecting shock structures which can be classified as regular or Mach reflections. The relationship between the approximately quadrupolar acoustic wave predicted by theory and the complex wave structure observed by Naumann and Hermanns is clarified by the results presented in this paper.

The production of noise is only one of the interesting features of the shock-vortex interaction. The mutual influence of shocks and vortices is fundamental to the mechanics of compressible turbulent flows. There are other aspects of the shock-vortex interaction besides the formation of acoustic waves that are important in the study of compressible flows. These include the linear and nonlinear shock distortion by the vortex flow field, including the development of diffracted, refracted, and transmitted shocks; and modification of the vortex flow field by passage of the shock, including amplification of the rotational motion.

In this paper, we present the results of two-dimensional numerical simulations of shock-vortex interactions. Our studies cover the development of a complex shock structure, the production of the acoustic waves observed experimentally, and the implications for shock turblence interactions. Previous work on this problem by Pao and Salas (11) used the two-step MacCormack scheme and dealt primarily with the quadrupolar acoustic wave structure

observed prior to the work of Naumann and Hermanns (3). Pao and Salas also presented a linear theory similar to the more detailed treatment of Ting (8). Zang et al. (12) have used similar methods to study the interactions of linear acoustic, entropy, or vorticity waves with a shock and of a shock with a temperature spot. Their primary interest was in the interaction of a shock wave with a turbulent boundary layer . Our interest follows from earlier studies of vorticity generation by shock-bubble (13) and shock-flame (14) interactions. Those calculations exhibited rearward propagating acoustic waves, shock diffraction and refraction by the bubble or flame, and merging of the various shocks to form a transmitted shock. We observe the same types of waves in the shock-vortex interaction.

The present calculations were performed on the Numerical Aerodynamic Simulation Program Cray Y-MP at the NASA Ames Research Center and on the TMC Connection Machine at the Naval Research Laboratory . The latter system is particularly convenient for flow visualization and has facilitated easy identification of the various acoustic wave structures that are produced by the shock-vortex interactions. Most of our work has involved the interaction of a planar shock with a single vortex or a vortex pair. The cases considered had a Mach number of either 1.05 or 1.5 in combination with a "weak" or "strong" vortex, as determined by the peak velocity in the vortex flow field. The single vortex interactions are examined for the production of acoustic waves. In order to relate our results more closely to the distortion of the planar shock by a turbulent field, we also investigate the interaction a pair of counter-rotating vortices.

The following section describes our numerical methods and initial conditions in detail. Then we discuss the shock structure resulting from the interaction of an initially planar shock with a vortex pair and suggest a simple linear model to predict shock distortion during the early phase of the interaction. Then we discuss the production of acoustic waves and their nonlinear interaction. Finally, the implications of our results on shock turbulence interactions are discussed.

Numerical Technique and Initial Conditions

Numerical Technique
The following equations for the conservation of mass, momentum, and energy density

3

$$\frac{\partial \rho}{\partial t} + \nabla \cdot (\rho \mathbf{V}) = 0 \tag{1}$$

$$\frac{\partial \rho \mathbf{V}}{\partial t} + \nabla \cdot (\rho \mathbf{V} \mathbf{V}) = -\nabla P \tag{2}$$

$$\frac{\partial E}{\partial t} + \nabla \cdot (E \mathbf{V}) = -\nabla \cdot (P \mathbf{V}) \tag{3}$$

are solved where ρ is the mass density, $\mathbf{V}$ is the velocity vector, P is pressure, and E is the total energy density The relation between internal energy, e, and pressure is given by

$$e = \frac{P}{\gamma - 1} \tag{4}$$

where γ is the ratio of specific heats. Temperature (T) is introduced through the thermal equation of state,

$$P = nkT \tag{5}$$

where n is the number density and k is the Boltzman constant. This set of equations is rewritten in terms of finite-difference approximations on an Eulerian mesh. The solution to the convection of conserved quantities is obtained with the Flux-Corrected Transport (FCT) algorithm which is an explicit, finite-difference algorithm with fourth-order phase and amplitude accuracy. FCT has been used for *computations of supersonic flows* and extensive comparison to theory and experiment have been made (15,16).

Initial conditions

Figure 1 shows the computational domain for the simulations of a shock interacting with a vortex pair. The domain is 20 x 10 cm^2 and consists of a 480 x 240 uniform grid. The initial position of the shock is x = 4 cm. Air flows through the left boundary at a fixed velocity, temperature, and pressure such that a shock propagates from the left to the right. The top and bottom boundaries are reflecting. The right boundary is open.

Results for two different shocks interacting with either a vortex pair or a single vortex are presented in this paper. The strong shock has a Mach number of 1.5, a pressure ratio of 2.45, and a density ratio of 1.86. The weak shock has a Mach number of 1.05, a pressure ratio of 1.1196, and a density ratio of 1.0839. The timesteps for the weak and strong shock simulations were 0.43 and 0.29 microseconds, respectively. In the simulations of a

4

vortex pair, the flow field consists of a pair of counter-rotating isothermal composite vortices. A composite vortex consists of an inner core of uniform vorticity with total circulation Γ and an outer annular region of uniform and oppositely directed vorticity with total circulation $-\Gamma$. For the single vortex problem, the velocity is counterclockwise in both regions and is described by

$$v_\theta = \frac{v_{max}}{r_1} r \qquad 0 < r < r_1 \tag{6}$$

and

$$v_\theta = Ar + \frac{B}{r} \qquad r_1 \leq r \leq r_2 \tag{7}$$

where v_{max} is the maximum velocity, occurring at $r = r_1$. Constants A and B are chosen such that the velocity matches that determined by equation 6 at $r = r_1$ and decays to zero at $r = r_2$. Outside of $r = r_2$, the velocity is zero everywhere. Since the range of influence of a composite vortex is finite, the boundaries do not affect the the vortex field. In addition, the shock and the vortex fields are totally isolated at $t = 0$. The initial pressure field is always specified such the pressure gradient balances the centripetal force,

$$\frac{dP}{dr} = \rho \frac{v_\theta^2}{r} \tag{8}$$

For the vortex pair problem, the upper vortex is this composite vortex and the lower vortex is identical except that v_{max} is opposite in sign resulting in a clockwise velocity field. The centers of the vortices are separated by a distance $2r_2$.

Simulations of the vortex without a shock indicate that the peak in the velocity profile at the edge of the central core decreases by approximately 2% within a few timesteps. After this time, the velocity and pressure fields of the vortex pair are constant. Simulations of the shock propagating through a quiescent gas show that after a few timesteps the shock thickness is 3 to 5 cells and then remains constant.

We investigated various values of r_1 and r_2 for the vortex. The size of the inner radius, r_1, has a significant effect on the flow field but the size of the outer annular region, $r_2 - r_1$, does not. We compared calculations with $r_2 = 2.75$ to those with $r_2 = 1.75$ for a strong

5

shock and a strong vortex. The ratio of the annular areas for these two cases is about 3.5:1. Both cases showed similar shock structure and vortex distortion. The peak pressure of the two cases was within 10%. We also assumed that the vortex was isothermal rather than isentropic.

In our calculations, the inner radius, r_1, and the outer radius, r_2, equal 0.75 and 1.75 cm, respectively. The maximum velocity, v_{max}, equals 230 m/s and 27 m/s for the strong and weak vortex pairs, respectively. These values of v_{max} were selected because they approximately equal the fluid velocity behind the strong and weak shocks.

A pressure profile through the center of the upper vortex is shown in Figure 2 for each of the four cases that we studied:

      1. a pair of weak composite vortices interacting with a weak shock,
      2. a pair of weak composite vortices interacting with a strong shock,
      3. a pair of strong composite vortices interacting with a weak shock,
      4. a pair of strong composite vortices interacting with a strong shock.

In addition, we present calculations of a single vortex interacting with a shock. In these simulations the single vortex is rotating in the counterclockwise direction. The computational domain is 20 x 20 cm^2 and consists of a 512 x 512 grid. The two simulations of a single vortex are

      5. a strong composite vortex interacting with a weak shock, and
      6. a strong composite vortex interacting with a strong shock.

Results

Experimental results (1-3) have shown that both the vortex and the shock respond to the interaction. In the following subsections, we discuss the shock structure and the production of acoustic waves. We also relate our results to shock-turbulence interactions.

Shock Structure

When a shock contacts a boundary, the resulting shock structure depends upon the particular characteristics of the interaction. The most familiar example of this is a shock diffracting over a wedge where the wave structure may be classified as either a regular

reflection or a Mach reflection depending upon the wedge angle and the shock strength. Similarly, Sturtevant and Kulkarny (17) observed that a focused shock may develop two different wave structures depending on the aperture of convergence and the shock strength. In our simulations, we also observe two different structures depending on the vortex strength and the shock strength.

The structure of a strong shock interacting with a strong vortex is illustrated in figure 3. During the early stage of the interaction (figure 3a), the upper portion of the shock is diffracted around the vortex. The shock velocity is opposed by the vortex rotation and, consequently, this shock is propagating more slowly than the shock which is diffracted around the lower half of the vortex. The two diffracted shocks are connected by the refracted shock which passes through the center of the vortex. At later times, the front consists of two connected Mach structures (figure 3b) each of which is similar to the structure of a Mach reflection. The first reflected shock (R1) is disconnected from the vortex and is propagating at a greater velocity than the second reflected shock (R2) which is still diffracting around the vortex. The two incident shocks (I1 and I2) and the Mach stem (MS) form the transmitted shock at later times. In the interaction of a shock with a vortex pair, each vortex produces this shock structure.

The structure of a weak shock interacting with a strong vortex is similar to the structure of a regular reflection of a shock propagating over a wedge. There is no Mach stem and the reflected shocks, R1 and R2, and the two branches of the incident shock , I1 and I2, all meet at the same point. This distinction between the strong and weak shock behavior agrees with the experimental observations of Naumann and Hermanns (3) for shock-vortex interactions.

When the vortex is weak, the shock front is distorted but a complex shock structure does not develop. This situation is typical of that described in theoretical analyses which assume only small perturbations to the planar front.

We present four typical cases of shock distortion. In two cases, the weak shock interacting with the weak vortex, and the strong shock interacting with the strong vortex, the maximum velocity in the vortex (v_{max}) is approximately equal to the fluid velocity (v_f)

behind the shock ($v_{max} = v_f$). The other two cases, the strong shock interacting with the weak vortex ($v_{max} \ll v_f$) and the weak shock interacting with the strong vortex ($v_{max} \gg v_f$) represent the extremes of shock distortion.

Weak vortex pair - strong shock ($v_{max} \ll v_f$)

A weak vortex pair has only a minimal effect on a strong shock as illustrated in figure 4. The shock is slightly curved as it passes over the vortex and remains thin throughout the simulation. The pressure jump is constant and equal to its original value.

Weak vortex pair - weak shock ($v_{max} = v_f$)

The weak vortex pair interacting with the weak shock is shown is figure 5. The maximum velocity of the vortex is roughly equal to that of the fluid behind the shock, The shock distorts only slightly as it passes over the vortex pair. The shock is slightly curved and the shock jump is not constant along the front. The maximum pressure along the shock front increases by 20% as it interacts with the vortex. By t=0.215 ms, the front is once again planar. There are small variations in the pressure field behind the shock throughout the simulation.

Strong vortex pair - weak shock ($v_{max} \gg v_f$)

Figure 6 shows a time sequence of pressure difference contours for a strong vortex pair and a weak shock. The difference in local fluid velocity significantly distorts the shock front as it passes over the vortex pair. At t=0.0215 ms, the planar shock is just outside the vortex flow field. At t=0.0645 ms, the shock is diffracting around each vortex and the shock structure is similar to that shock in Figure 3a. The refracted shock (RF) thickens as it passes through the vortex. At t = 0.1075 ms, the t ansmitted shock has propagated beyond the vortex field. For this weak shock interaction, the structure is similar to a regular reflection . There is no Mach stem and the two branches of the incident shock (I1 and I2 in figure 3b) and the two reflected shocks (R1,R2) meet at the same point where a pressure peak has formed. In addition, there is a pressure peak at the centerline of the computational domain where the incident shocks intersect. From t=0.1505 ms, the shock propagates through the flowfield. The shock (R1) reflects from the upper and lower walls. Finally, the shocks merge into a single curved front at t=0.3225 ms.

We considered several models to predict the shock deformation and identified both a linear and a nonlinear regime of interaction. In the linear regime, the shock curvature is predicted well by the convection of a particle interface as shown in Figure 7. At t = 0 ms, the interface is an array of 100 particles which coincides with the initial location of the shock. The particle velocity vector V_p is

$$V_p = V_s + V_v \tag{9}$$

where V_s is a constant equal to the velocity of the shock in the unperturbed fluid and V_v is the local fluid velocity vector due to the vortex pair. At t=0.0645 ms, the refracted shock has been thickened due to its interaction with the vortex and the leading edge is drawn in the figure. The particle interface is indistinguishable from the shock until t=0.086 ms. The model accurately predicts the shock curvature while the shock is within the rotational field of the vortex. At later times, however, as the complex shock structure develops, the model fails because the assumption of a constant shock velocity is no longer valid.

The shock velocity is not constant after the interaction because the pressure jump varies along the shock front. The relationship between the shock jump and the shock speed is discussed by Whitham (18). His theory of two-dimensional shock propagation includes the non-linear effects of gas dynamics in which the shock speed is not constant but increases with the local pressure. This implies that the propagation speed varies along the shock front. As a concave shock is focused inward and the local pressure behind the shock increases, the local propagation speed of the shock also increases. For a shock with a continuously varying curvature, the more concave regions are accelerated while the more convex regions are decelerated. In our calculations, the acceleration of the shock is significant only after it propagates out of the vortex flow field.

Strong vortex pair - strong shock ($v_{max} = v_f$)

These conditions are similar to those of the weak shock and weak vortex because the velocity behind the shock is equal to the maximum velocity in the vortex. In this case, however, the velocity equals 230 m/s and the interaction is much stronger, as illustrated in Figure 8. The shock enters the vortex flow field and begins to distort at t=0.435 ms. The curved shock consists of the diffracted shocks propagating around the outside of the vortex pair and the refracted shocks which are propagating through the vortex flow field, as

9

illustrated in figure 3a. Pressure peaks begin to form on the outside of the vortex pair where the slow diffracted shock (SD) and refracted shock (RF) intersect. At t=0.0725 ms, the shock is emerging from the vortex pair flow field. The transmitted shock has accelerated out of the high pressure regions to form the connected Mach structures as in figure 3b. For the remainder of the simulation, the Mach stem accelerates with respect to the incident shock and finally at t=0.2175, the front is approximately planar.

Figure 9 shows the convection of a particle interface for the interaction of a strong shock and a strong vortex pair. The particle interface coincides with the shock until t=0.058. At later times, the acceleration of the highly concave portion becomes important and the shock velocity is no longer approximately constant.

Production of Acoustic Waves

The nonlinear regime is characterized by the formation of secondary waves. Experiments on shock-vortex interactions have concentrated on these waves which are generally identified as acoustic waves propagating upstream. Although the secondary waves are apparent in the vortex pair calculation, they interact with the walls and the analysis is somewhat more complicated. Therefore, we present simulations of a single vortex in a larger computational domain as described in the Initial Conditions.

As noted in the Introduction, experimental observations indicate the formation of an acoustic wave when a shock interacts with a single vortex. Theoretical analysis indicates that the acoustic wave is quadrupolar although experimental observations show a strong compressive region attached to the shock front. The simulations presented here show the relationship between this strong compression and the quadrupolar wave.

The formation of the cylindrical acoustic wave occurs in two stages. In the first stage, a quadrupole pressure field develops behind the shock. In the second stage, the propagating shock distorts due to its interaction with the vortex and a complex shock structure forms. For a strong shock, the reflected shock (R1 in figure 3b) propagates faster than the quadrupole and merges with the quadrupole to produce an asymmetric pressure distribution around the cylindrical wave.

10

Strong vortex - weak shock

This two-stage process is most obvious in the interaction of the strong vortex with the weak shock as illustrated in figure 10. In figure 10c, a weak quadrupole is propagating outward from the center of the vortex. The radius ($r = R_q$) indicates the approximate location of the outer boundary of the quadrupole. The pressure distribution around the circumference of this arc is shown next to the figure. The expansion and compression regions are weak but approximately equal in magnitude. Also at this time, the shock is distorting and the reflected wave (R1 in figure 3b) at $r = R_r$ is propagating outward. The pressure distribution around this arc indicates a strong compression region attached to the shock front. At later times, these two waves propagate radially outward (figure 10d-f). In this case, the strength of the reflected wave is approximately equal to that of the quadrupole and the two do not merge. The interaction of a strong vortex with a weak shock could not be observed by either Dosanjh and Weeks (2) or Naumann and Hermanns (3). In those experiments, the passage of the shock over an airfoil created a starting vortex. After reflection from the endwall, the planar shock interacted with the vortex. The maximum velocity of a vortex created in this manner could never exceed the fluid velocity behind the shock.

Strong vortex - strong shock

The interaction of a strong vortex with a strong shock is illustrated in figure 11. In this case, the cylindrical acoustic wave is quite apparent. The two-stage formation of the acoustic wave is illustrated in figure 12. These initial conditions are similar to those of Dosanjh and Weeks (2) and in this case the reflected shock merges with the quadrupole. In Figure 12b, the shock is passing over the vortex and the quadrupolar pressure field develops behind the shock. The arc at $r=r_q$ indicates the approximate boundary of the quadrupole. The pressure distribution around this arc shows that the compression and expansion regions are approximately equal in magnitude as predicted by the theory. The reflected shock (R1) is evident in figure 12b as a small arc at $r=r_r$ inside the quadrupole on the lower right. At later times (figure 12c-d), the reflected shock begins to overtake the quadrupole. In the final two frames (Figures 12e-f), the reflected shock merges with the quadrupole and the final pressure distribution shows the strong compression region attached to the shock front.

11

Insights into turbulence

The interaction of a shock with a vortex pair is a simple paradigm for shock-turbulence interactions. In this section we discuss two issues related to these interactions: the compression of the vortex flow field and the amplification of vorticity.

Weak vortex pair - strong shock

Figure 13 shows the vorticity contours for a weak vortex pair and a strong shock. At t=0, the upper vortex consists of a central core of positive vorticity with a concentric ring of negative vorticity. The lower vortex is identical except that the signs of the vorticity are reversed. As the shock interacts with the vortex at t = 0.0725, the vorticity field appears noisy due to the low velocity gradients in the flow. The shock compresses each vortex into an ellipse with the major axis equal to the original radius of the vortex (figure 13d-f). This agrees with the experimental observations of Dosanjh and Weeks (2). Although the vorticity is small, it remains confined to the region defined by the compressed vortex pair. Each vortex is rotating about its central axis, but the time interval shown is so short that the rotation is not evident.

Strong vortex pair - strong shock

The strong vortex pair is significantly affected by its interaction with the strong shock, as illustrated in figure 14. The shock compresses the vortex as it passes through the rotational flow field (figure 14b-c). At t=0.1015 ms, the vortices are not smooth ellipses. The regions of positive and negative vorticity are beginning to separate as each vortex rotates about its axis. At t=0.2175 ms, the regions of positive and negative vorticity are no longer concentric rings but are separate regions. The inner core of vorticity is an elongated strip with vorticity of opposite signs on either side.

The pressure field (Figure 8) of the vortex pair does not respond as quickly to the interaction as the vorticity. At t=0.0725 ms, each vortex is round with pressure peaks on the outside of each vortex. The pressure field of each vortex begins to distort at t=0.1015 ms. At later times, the pressure field indicates that the vortices are elliptical. By t=0.1595 ms, each vortex has rotated approximately one-quarter turn since the beginning of the

12

simulation, and its major axis is now roughly aligned with the streamwise flow. In the final frame the pressure gradient has steepened further on the outside edge of the vortex.

In a steady-state axisymmetric vortex, the pressure gradient balances the centripetal force as indicated in equation 8. When the local pressure field of the vortex is distorted, this balance is perturbed and the velocity, density, and pressure field readjust to a new steady-state. In this problem, the interaction time between the shock and the vortex pair is much less than a typical fluid dynamic time scale such as the time for a complete rotation of the vortex. The vortex pair is unstable as soon as the shock passes and it requires one to two rotations in order to reach a new steady-state configuration. We continued this calculation in order to determine the final state of the vortex pair. After the shock passes, the vortex pair is convected with the fluid velocity of approximately 230 m/s. At this velocity, the vortex pair would have convected beyond the calculational domain before reaching a steady-state. Therefore, we shifted the domain every 0.0145 μs from t=0.232 to t=0.348 μs. Twenty computational cells were subtracted from the left side of the domain and added to the right side in front of the shock. By t=0.348 μs, the shock was sufficiently far from the vortex and it propagated out of the computational domain.

Figure 15 shows contours of pressure difference and vorticity after the vortex pair has reached a steady state at t=0.580 ms. The density and pressure gradients in each vortex are steeper than those in the original isothermal vortex pair. Each vortex is once again round but smaller due to the interaction with the shock. These observations agree qualitatively with those for a spiral vortex which show a decrease in the central core radius and a greater density difference after it has passed through a shock (2). The vorticity contours show that the inner core of vorticity is round and that vorticity of opposite sign is distributed asymmetrically around the central core.

In shock-turbulence problems, a typical measure of the strength of the interaction is the change in the turbulent kinetic energy. In our problem, the initial vortex flow field is constant and therefore, there are no turbulent fluctuations. We are however, still interested in the change in the vorticity distribution which can be related to turbulent flows.

13

When a shock interacts with a vortex, the vorticity field changes as a result of two separate phenomena. Vorticity is produced due to the baroclinic term, $\nabla\rho \times \nabla P/\rho^2$ and it is redistributed due to compression. An integral measure of the change in vorticity, ξ, is the enstrophy

$$E = \int_A \xi^2 \, dA \tag{7}$$

where A is the area of the domain. The enstrophy, nondimensionalized by its initial value, is shown in Figure 16 as a function of time for all four cases studied. The enstrophy is constant when a weak shock interacts with either a weak or a strong vortex. But when a strong shock passes over the vortex, the enstrophy increases significantly and then remains fairly constant for the remainder of the calculation. The increase in enstrophy for the weak vortex is proportionately greater than that for a strong vortex.

As a shock passes over a vortex with a pressure and density gradient, vorticity of opposite signs is produced in the upper and lower halves of the vortex. If the production of vorticity is significant, the vortex will not remain symmetric about its centerline. The vortices in our calculation are symmetric which suggests that the production of vorticity is not significant in any of our simulations. In addition, we estimated that the vorticity produced from the baroclinic term for the strong vortex interacting with the strong shock is only a few percent of the vorticity in the core of the vortex. For all other cases, the vorticity production is even smaller. This implies that the enstrophy increases due to compression of the vortex and redistribution of the vorticity and not due to the net production of vorticity.

Conclusions

In this paper, we present simulations of a shock interacting with either a vortex pair or a single vortex. Shock structure and the production of acoustic waves are discussed for different shock and vortex strengths. In addition, the results are related to shock-turbulence interactions.

The simulations show that a shock is not significantly distorted by its interaction with a weak vortex. The interaction of shock with a strong vortex, however, produces a complex shock structure. Two different structures are observed and may be classified as either a regular reflection or a Mach reflection for a weak or a strong shock, respectively. This complex shock structure is closely related to the formation of the asymmetry in the acoustic wave pressure distribution.

The simulations also clarify the process by which acoustic waves are produced when a shock interacts with a single vortex. Experiments have shown that the interaction produces a cylindrical acoustic wave, but theoretical analyses fail to predict the pressure distribution around the wave without empirically derived parameters. The major discrepancy between the experiments of Hollingsworth and Richards (1) and the theory of Ribner (5,6) was the form of the cylindrical wave. The theoretical predictions showed that the wave was quadrupolar with the compression and expansion regions of equal magnitude. In contrast, the experiments revealed a wave with an intense compression region attached to the propagating shock front. The acoustic wave consists of two components: a quadrupole and a reflected shock. The initial interaction of the shock with the vortex produces a quadrupolar wave. But, in addition, the distortion of the initially planar shock produces a system of curved, reflected shock structures. For the strong shock interaction, the reflected shock eventually merges with the quadrupole resulting in an acoustic wave consisting of a stronger compression region attached to the shock front.

Finally, the calculations show that a strong shock compresses each of the vortices in a counter-rotating pair into an ellipse. The major axis of the ellipse is equal to the original radius of the vortex. The time required for the weak vortex pair to return to a steady state is quite long. The strong vortex pair recovers more quickly and finally consists of round vortices with a smaller diameter than the original vortex pair. When a shock interacts with the vortex pair, vorticity may be redistributed due to compression or it may be produced due to the interaction of the pressure and density gradients as described by the baroclinic term in the vorticity equation. In our simulations, the production term is quite small but the redistribution effect is significant for those interactions with a strong shock. The enstrophy, which is an integral measure of the change in vorticity, is constant for the interactions of a vortex pair with a weak shock. For a strong shock, however, the enstrophy increases significantly for the both the weak and strong vortex pairs.

15

Acknowledgements

References

1. M. A. Hollingsworth and E. J. Richards, ``A Schlieren Study of the Interaction between a Vortex and a Shock Wave in a Shock Tube,"*Aeronautical Research Council Fluid Motion Subcommittee Report A.R.C.*, F. M. 2323} (1955). I

2. D. S. Dosanjh and T. M. Weeks, ``Interaction of a Starting Vortex as Well as a Vortex Street with a Traveling Shock Wave," *AIAA J.* 3, 216 (1965).

3. A. Naumann and E. Hermanns, ``On the Interaction between a Shock Wave and a Vortex Field," in *Noise Mechanisms, AGARD CP-131,* 23-1 (1973). I

4. M. A. Hollingsworth and E. J. Richards, ``On the Sound Generated by the Interaction of a Vortex and a Shock Wave," Aeronautical Research Council Fluid Motion Subcommittee Report A.R.C. 18257, F. M. 2371} (1956).

5. H. S. Ribner, ``Convection of a Pattern of Vorticity through a Shock Wave," NACA Rept.1164 (1954)

6. H. S. Ribner, ``Cylindrical Sound Wave Generated by Shock-Vortex Interaction," *AIAA J.* 23, 1708 (1985).

7. T. M. Weeks and D. S. Dosanjh, ``Sound Generation by Shock-Vortex Interactions," *AIAA J.* 5, 660 (1967). I

8. L. Ting, ``Transmission of Singularities through a Shock Wave and the Sound Generation," *Phys. Fluids* 17, 1518 (1974).

9. M. J. Lighthill, ``On the Energy Scattered from the Interaction of Turbulence with sound or Shock Waves," *Proc. Camb. Phil.Soc.* 49, 531 (1953). I

10. H. S. Ribner, ``Spectra of Noise and Amplified Turbulence Emanating from Shock-Turbulence Interaction," *AIAA J.* 25, 436 (1987).

11. S. P. Pao and M. D. Salas, ``A Numerical Study of Two-Dimensional Shock Vortex Interaction," *AIAA 14th Fluid and Plasma Dynamics Conference Paper AIAA-81-1205* (1981).

12. T. A. Zang, M. Y. Hussaini, and D. M. Bushnell, ``Numerical Computations of Turbulence Amplification in Shock Wave Interactions," *AIAA 20th Aerospace Sciences Meeting Paper AIAA-82-0293* (1982).

13 J. M. Picone and J. P. Boris, *J. Fluid Mech.*189, 23 (1988).

14. J. M. Picone, E. S. Oran, J. P. Boris, and T.R. Young, Jr.,``Theory of vorticity Generation by Shock Wave and Flame Interactions," in *Dynamics of Shock Waves, Explosions, and Detonations, Vol.\ 94 of Progress in Astronautics and Aeronautics,* edited by J. R. Bowen, N. Manson, A. K. Oppenheim, and R. I. Soloukhin, (AIAA, New York, 1985), 429-448.

15. Boris, J.P., and D.L. Book, Solution of the continuity Equation by the Method of Flux-Corrected Transport, *Methods in Computational Physics* **16,** 85 (1976).

16. E.S. Oran and J.P. Boris, *Numerical Simulation of Reactive Flow,* Elsevier, N.Y.,NY (1987).

17. Sturtevant, B. and Kulkarny, V.A., "The Focusing of Weak Shock Waves," *J. Fluid Mech.***73,** 651 (1976)

18. Whitham, G.B., "A New Approach to Problems of Shock Dynamics,Part I: Two-dimensional Problems," *J. Fluid Mech.* **2,** 145 (1957).

1. Computational domain for calculations of a vortex pair interacting with a shock.

20 cm

10 cm
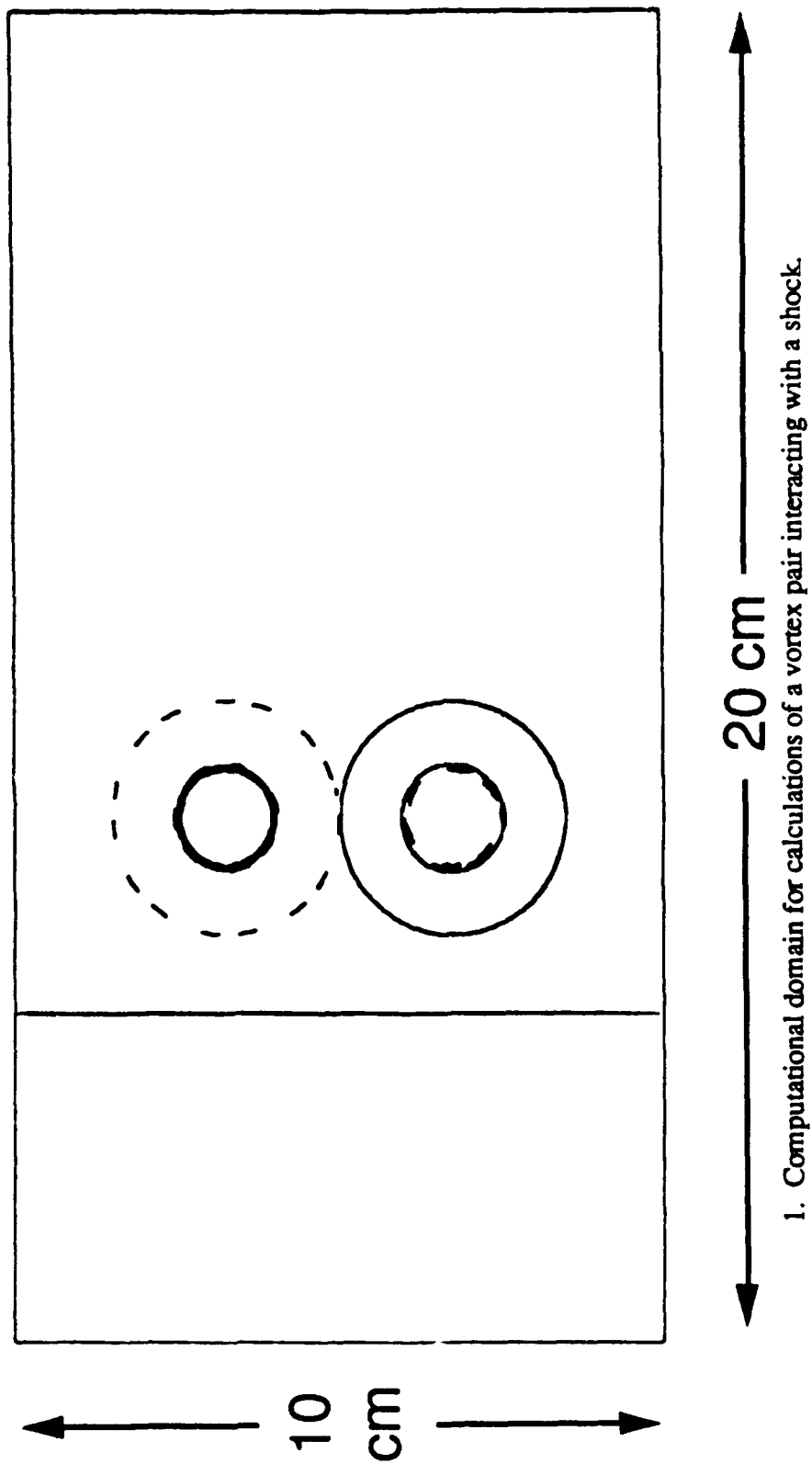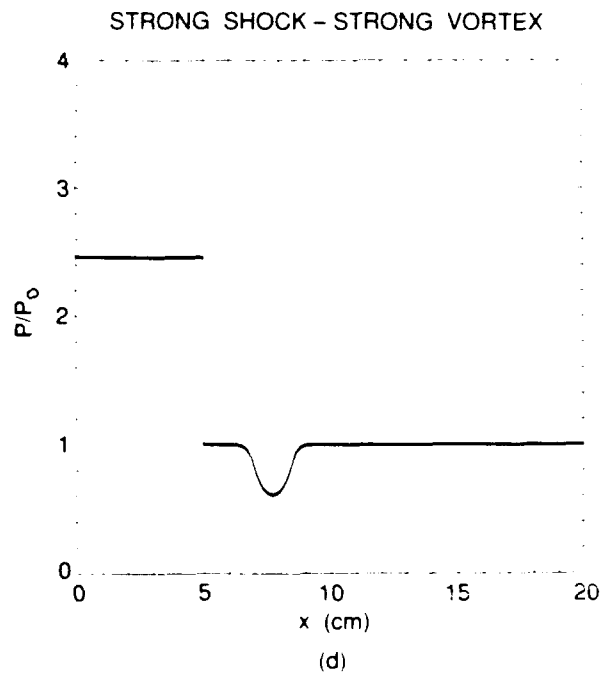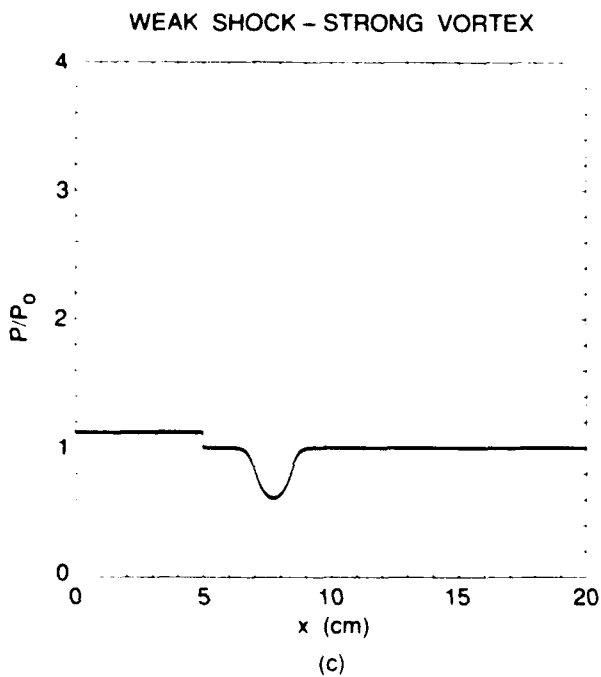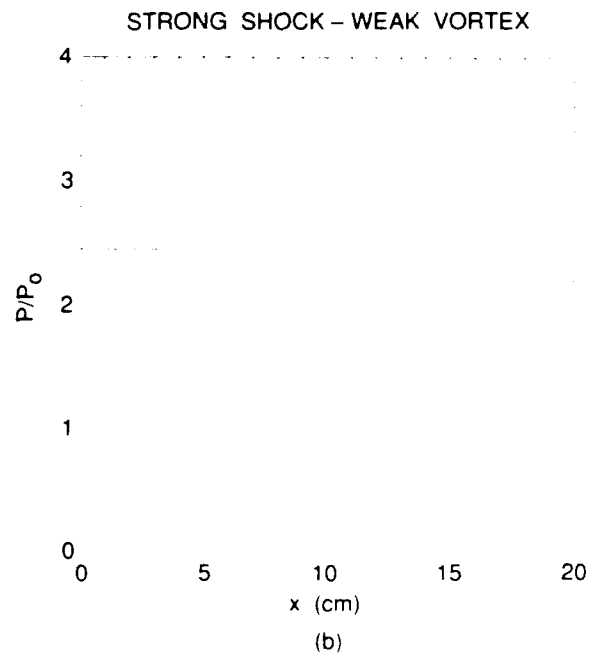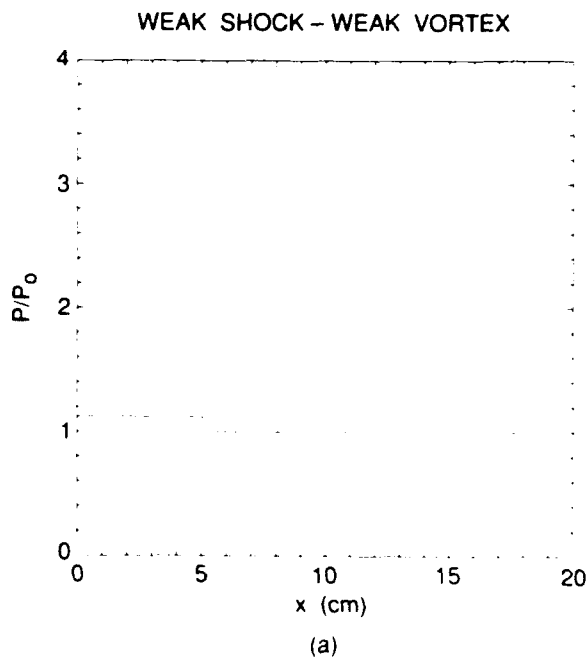
2. Pressure ratio through center of upper vortex at t=0 for (a) weak vortex and weak shock (b) weak vortex and strong shock (c) strong vortex and weak shock (d) strong vortex strong shock

(a)

(b)
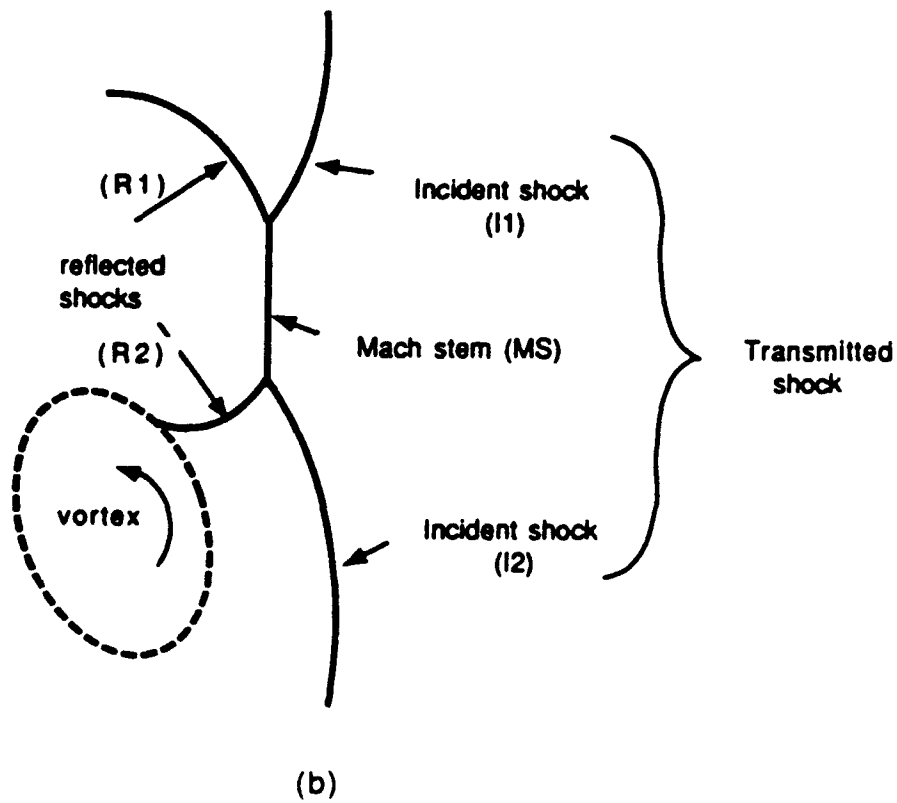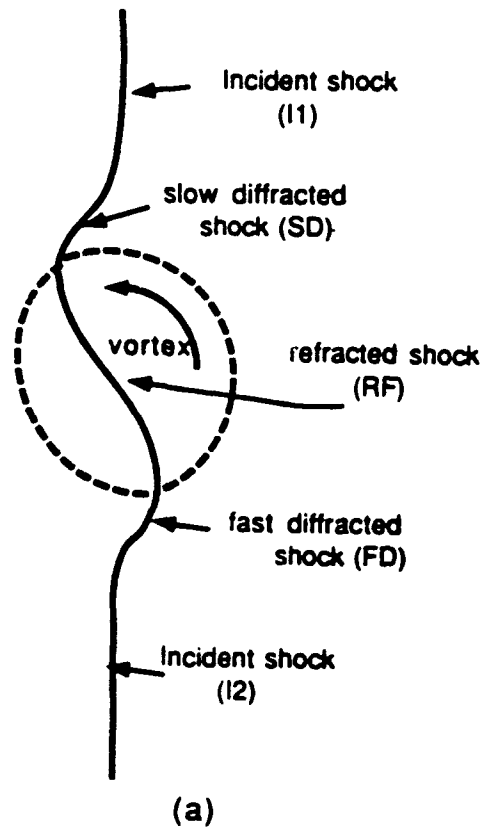
3. Complex shock structure during (a) early and (b) late stages of interaction.
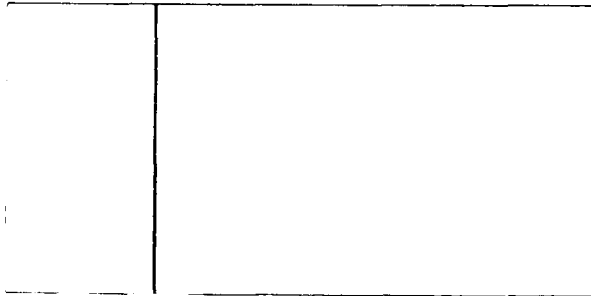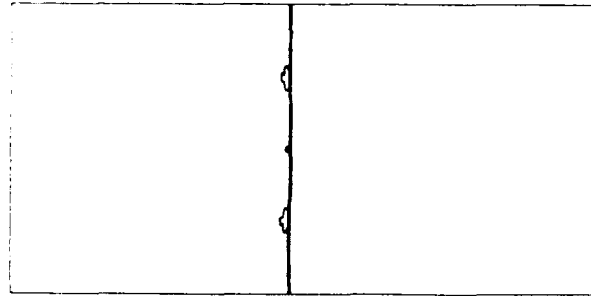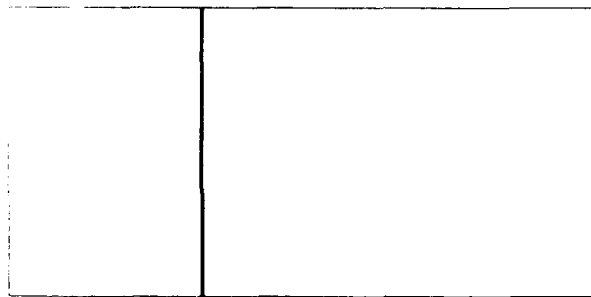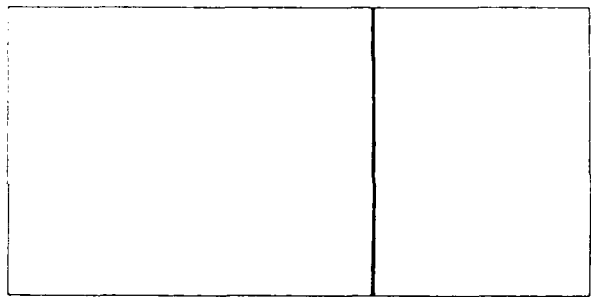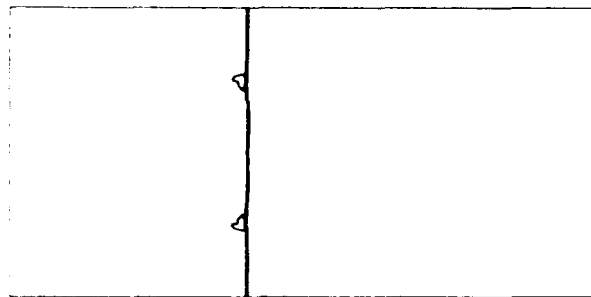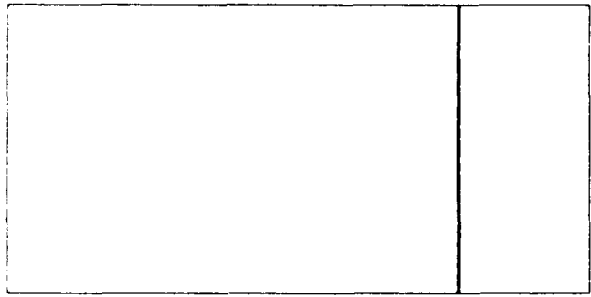
4. Pressure difference contours for weak vortex pair and strong shock at times (a) 0 (b) 0.029 (c) 0.058 (d) 0.087 (e) 0.145 (f) 0.203 ms. Contours range from -1.5e6 to -0.15e6 and 0.15e6 to 1.5e6 in intervals of 0.15e6.
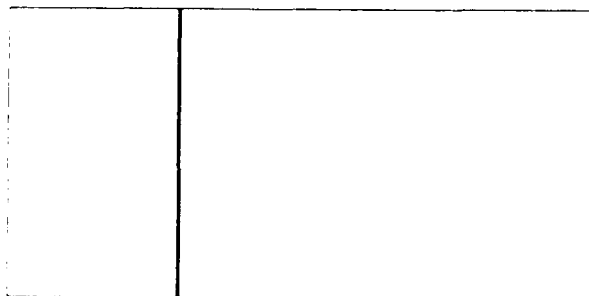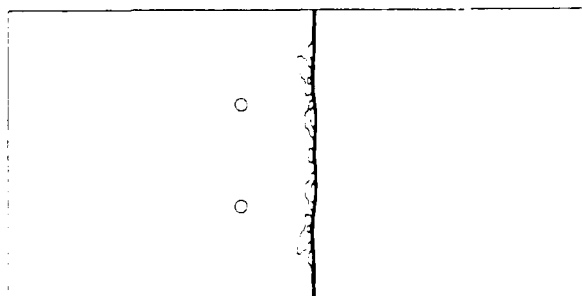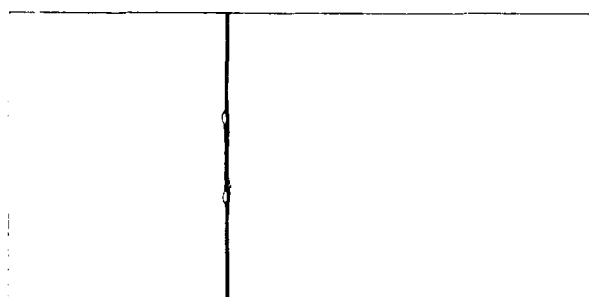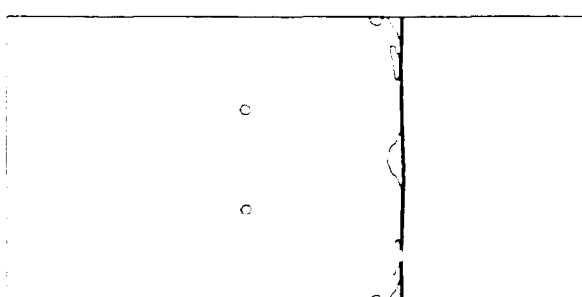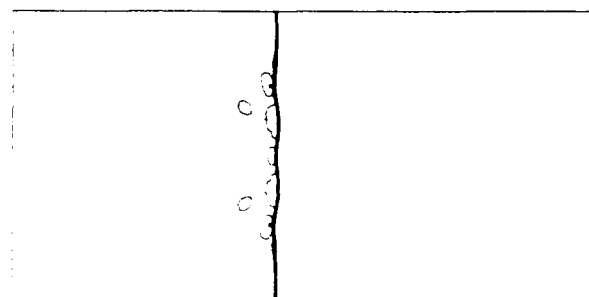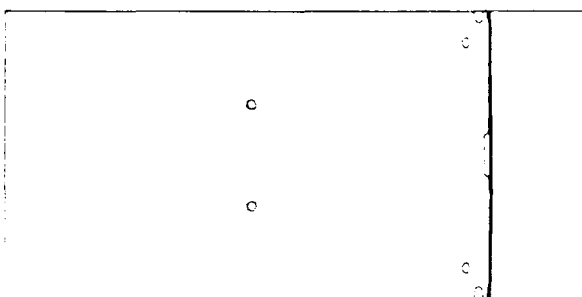
5. Pressure difference contours for weak vortex pair and weak shock at times (a) 0.0215 (b) 0.0645 (c) 0.1075 (d) 0.1505 (e) 0.2365 (f) 0.3225 ms. Contours range from -1.4e5 to -0.14e5 and from 0.14e5 to 1.4e5 in increments of -0.14e5.
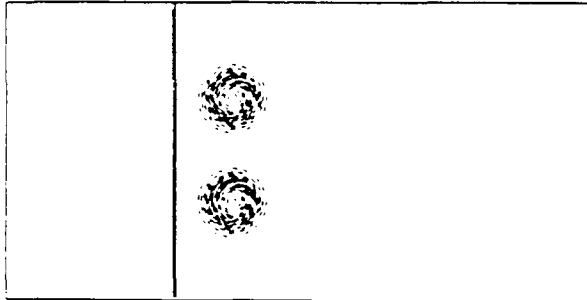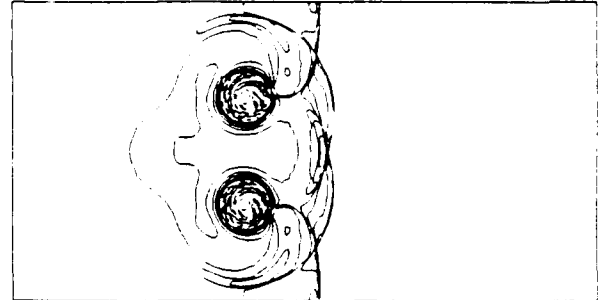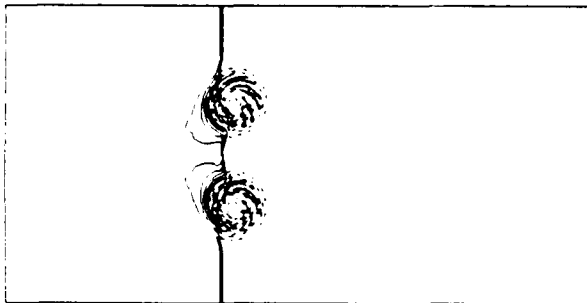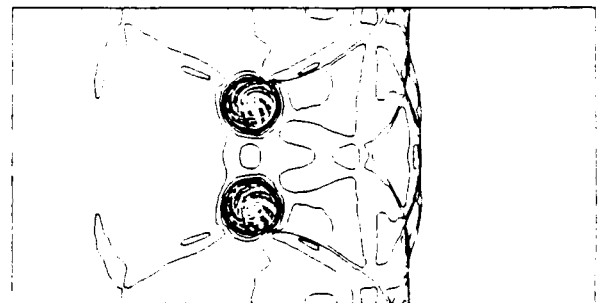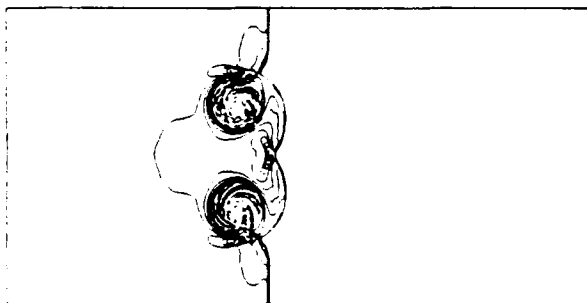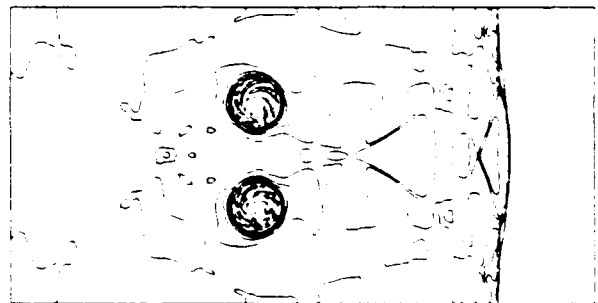
6. Pressure difference contours for strong vortex pair and weak shock at times (a) 0.0215 (b) 0.0645 (c) 0.1075 (d) 0.1505 (e) 0.2365 (f) 0.3225 ms. Contours range from -3.8e5 to -0.19e5 and 0.19e5 to 3.8e5 in intervals of 0.19e5.
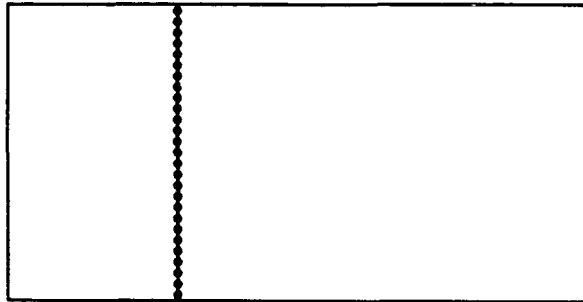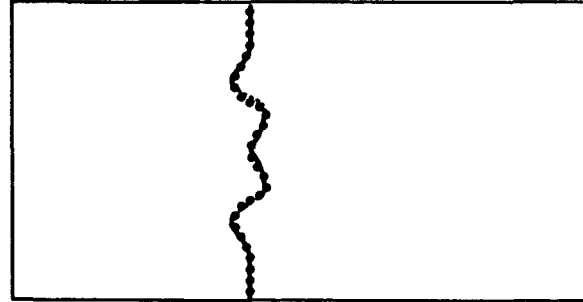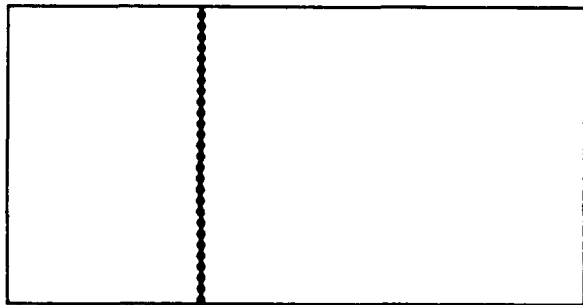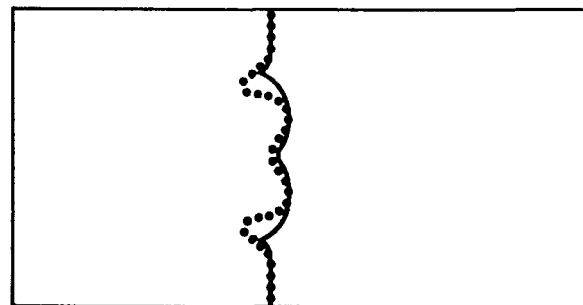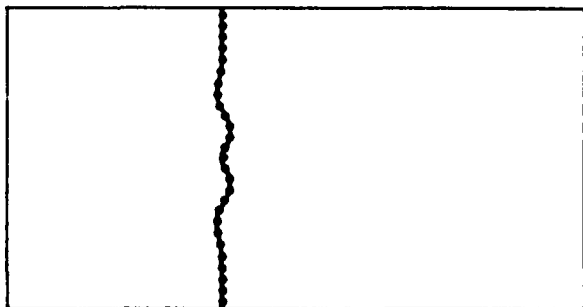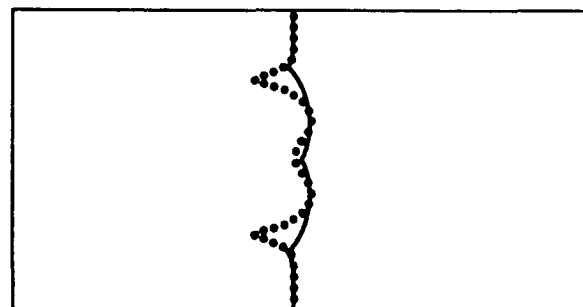
7. Comparison of shock distortion determined from simulation and from simplified model for strong vortex pair and weak shock at times (a) 0.0215 (b) 0.043 (c) 0.0645 (d) 0.086 (e) 0.1075 (f) 0.129 ms.
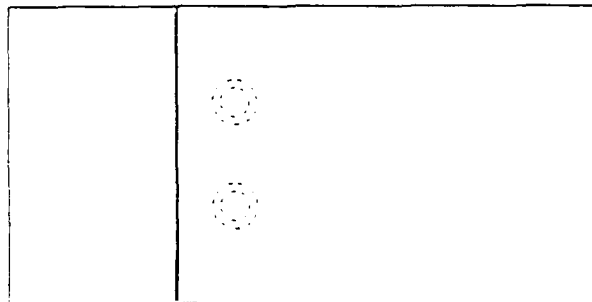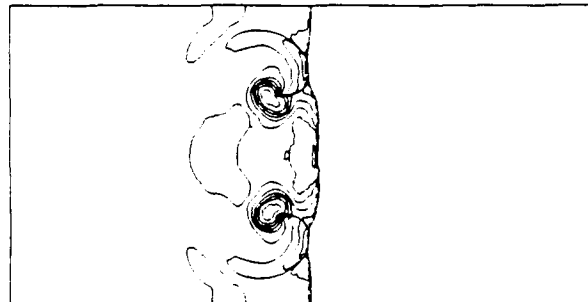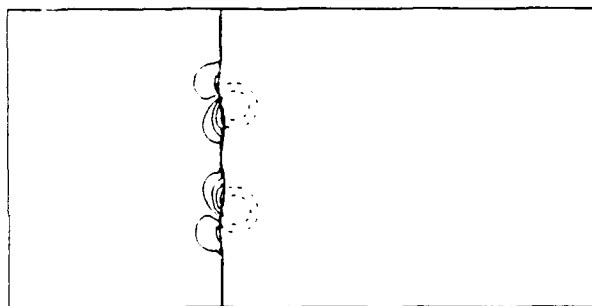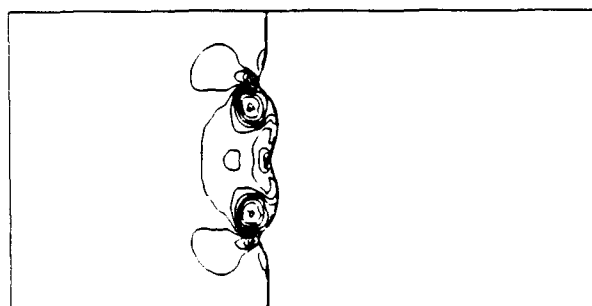
8. Pressure difference contours strong vortex pair and strong shock at times (a) 0.0145 (b) 0.0435 (c) 0.0725 (d) 0.1015 (e) 0.1595 (f) 0.2175 ms. Contours range from -2.85e6 to -0.15e6 and 0.15e6 to 2.85e6 in intervals of 0.15e6.
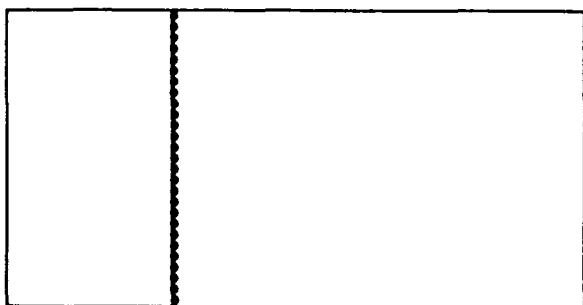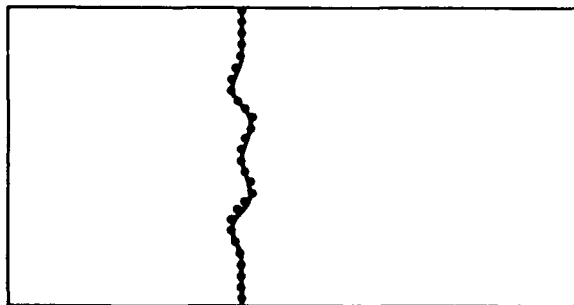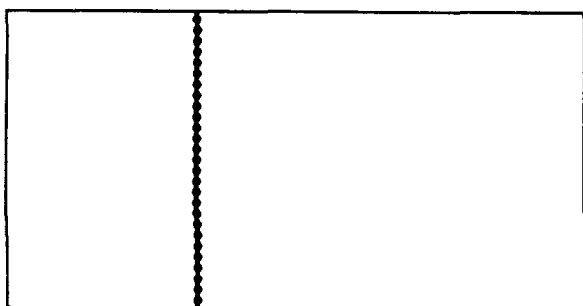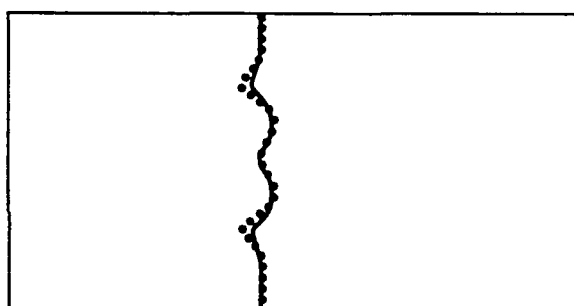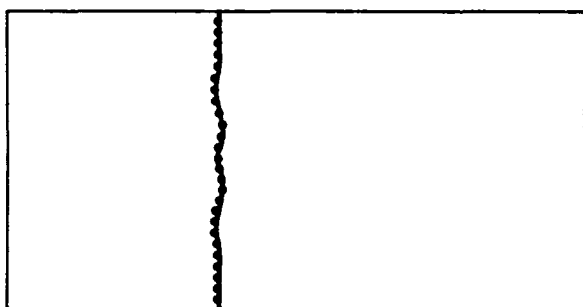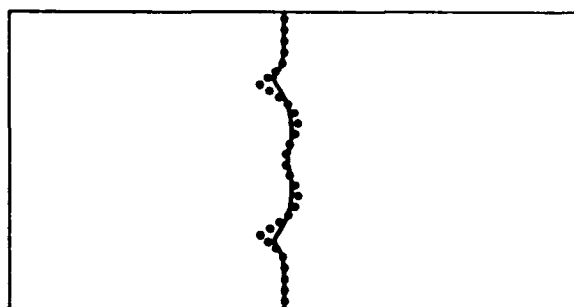
9. Comparison of shock distortion determined from simulation and from simplified model for strong vortex pair and strong shock at times (a) 0.0145 (b) 0.29 (c) 0.0435 (d) 0.058 (e) 0.725 (f) 0.087 ms.
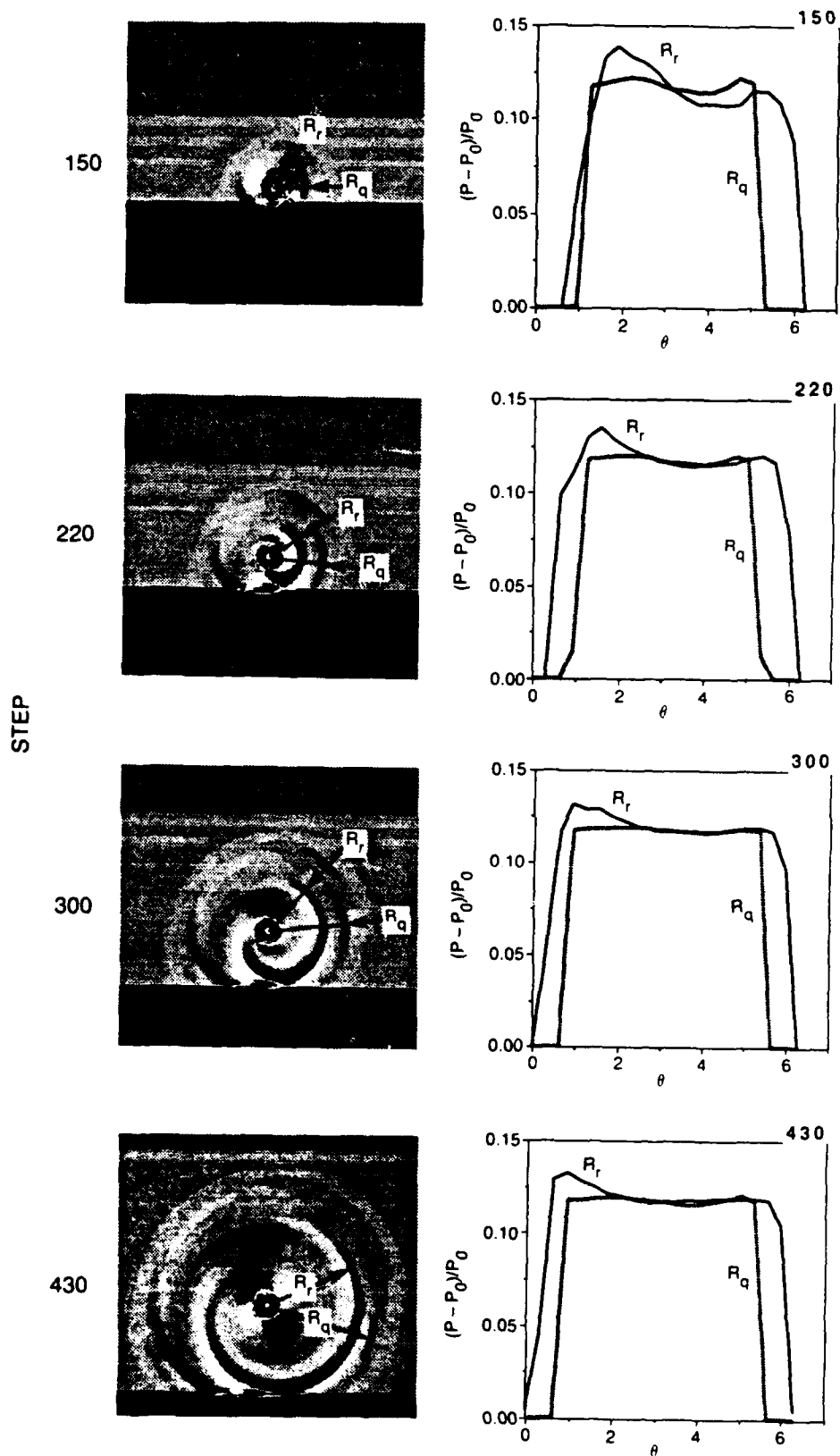
10. Pressure difference contours and pressure vs. θ at R_q and R_r for strong vortex and weak shock at times (a) 0 (b) 0.473 (c) 0.0946 (d) 0.129 (e) 0.1849 (f) 0.1849. $P_0 = 1$ atm.
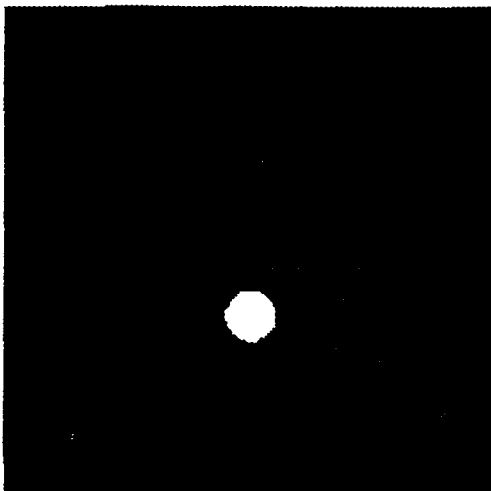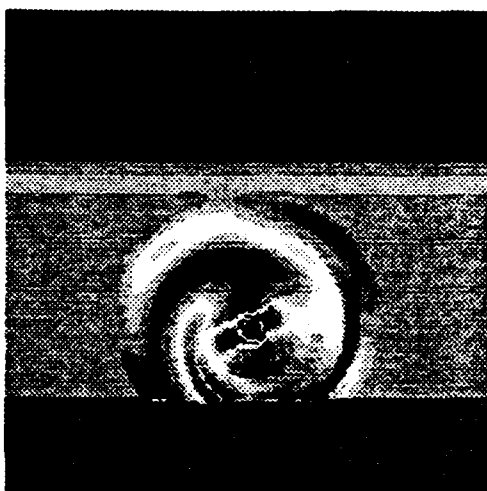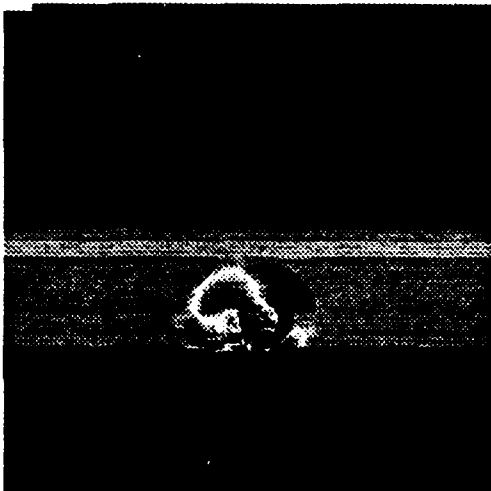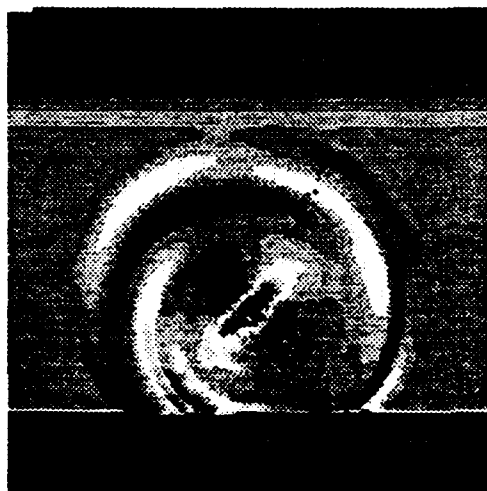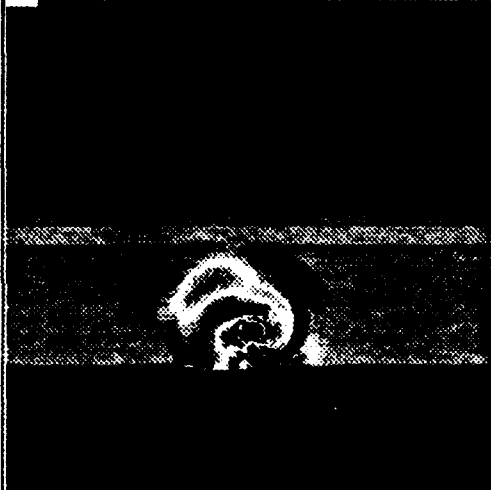
11. Pressure difference contours for strong vortex and strong shock at times (a) 0.00 (b) 0.05075 (c) 0.06525 (d) 0.10875 (e) 0.145 (f) 0.1856 ms .
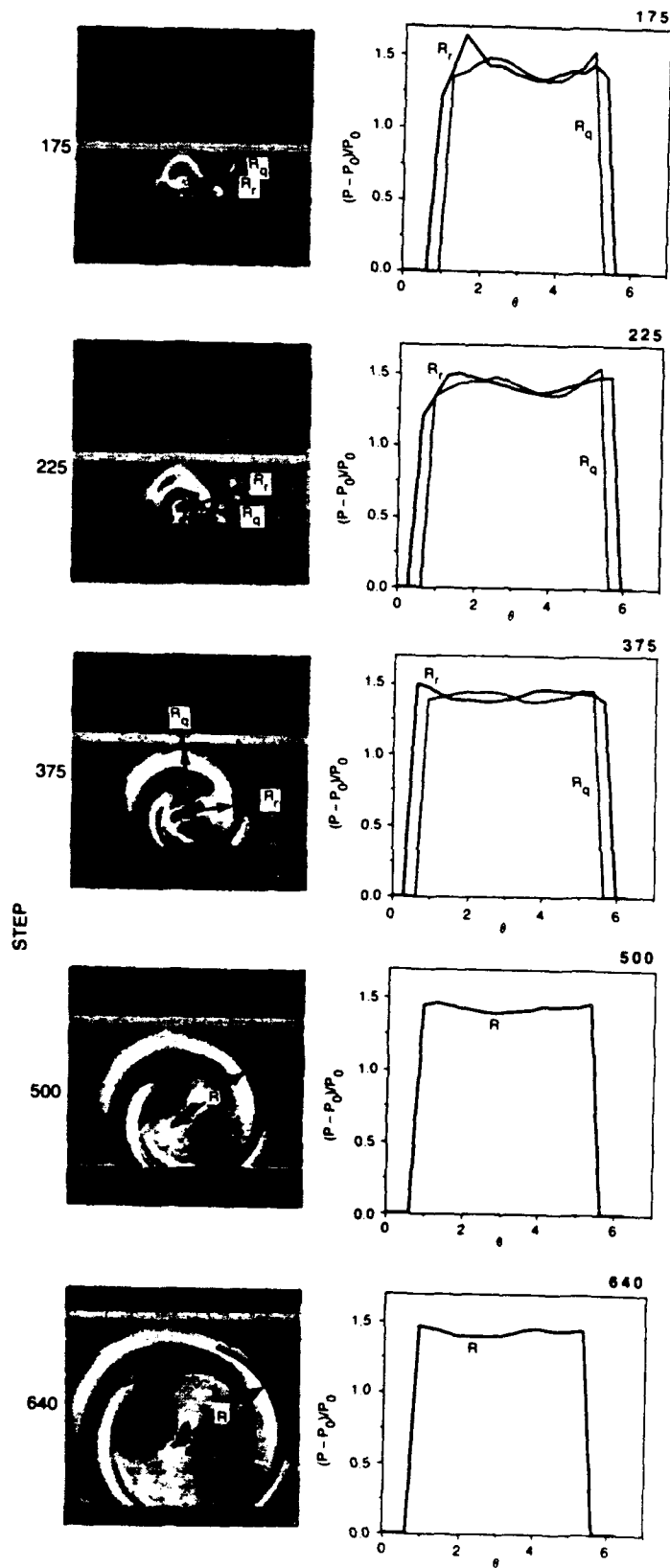
12. Pressure difference contours and pressure vs. θ at R_q and R_r for strong vortex and strong shock at times (a) 0.00 (b) 0.05075 (c) 0.06525 (d) 0.10875 (e) 0.145 (f) 0.1856 ms
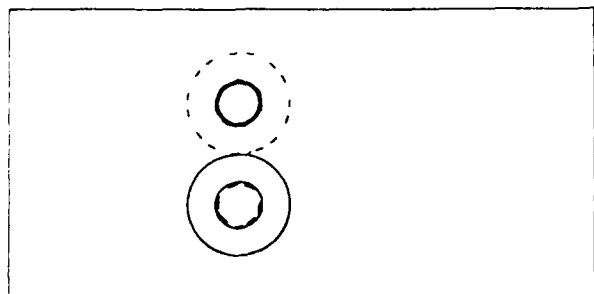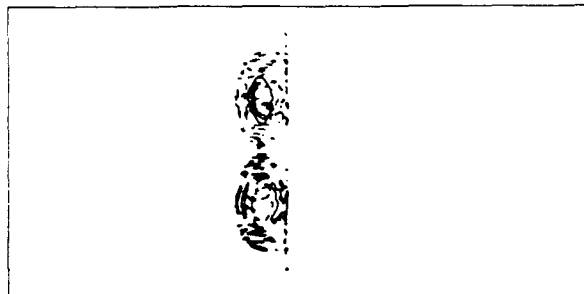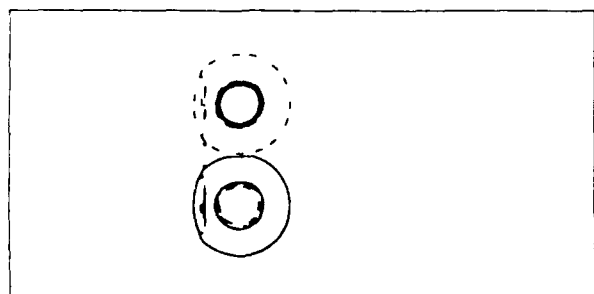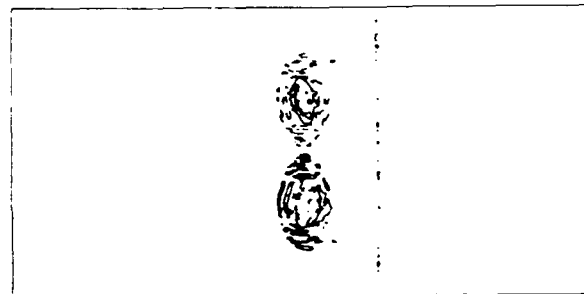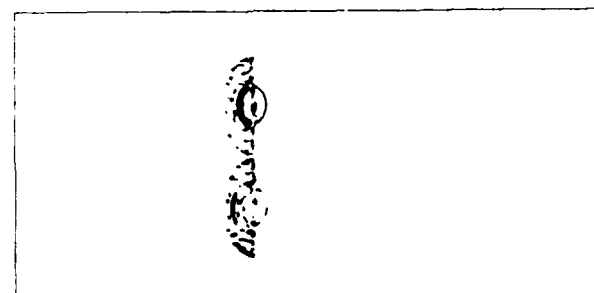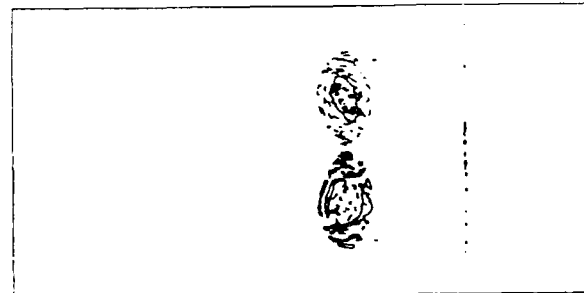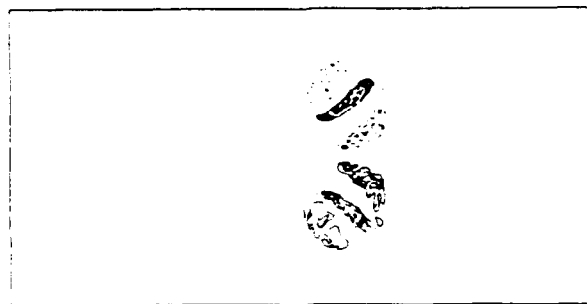
13. Vorticity contours for strong shock and weak vortex pair at time (a) 0.0145 (b) 0.0435 (c) 0.0725 (d) 0.1015 (e) 0.1595 (f) 0.2175 ms. Contours in (a) and (b) range from -10e3 to -1e3 and 1e3 to 10e3 in intervals of 3e3 s^{-1}. In (c) through (f), Contours range from -28e3 to -4e3 and 4e3 to 28e3 in intervals of 12e3 s^{-1}.
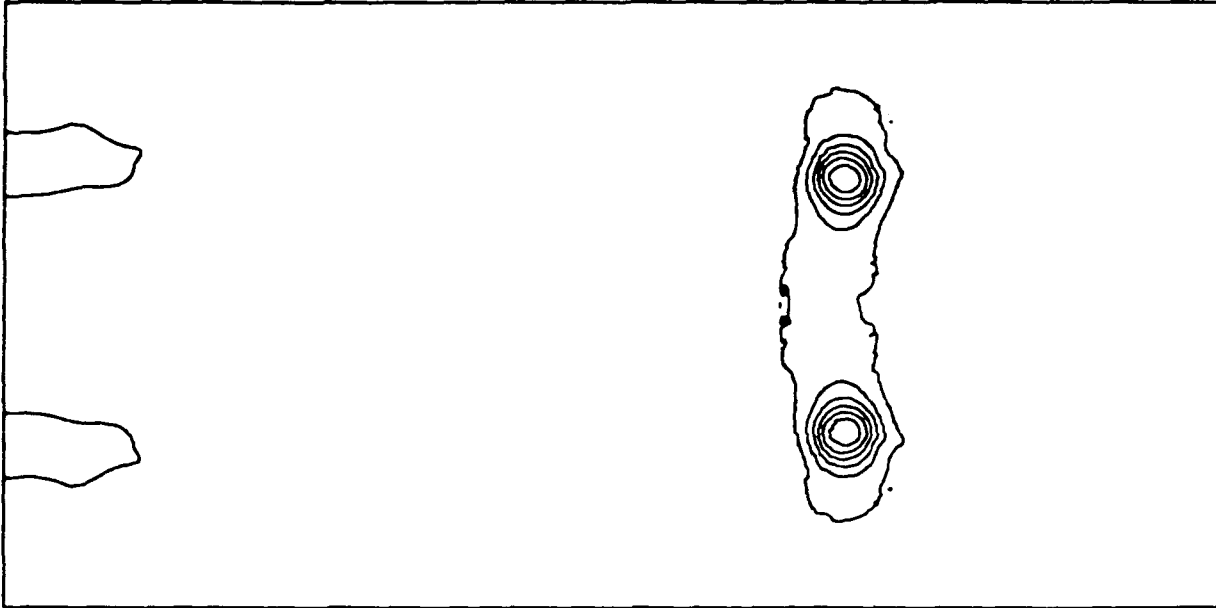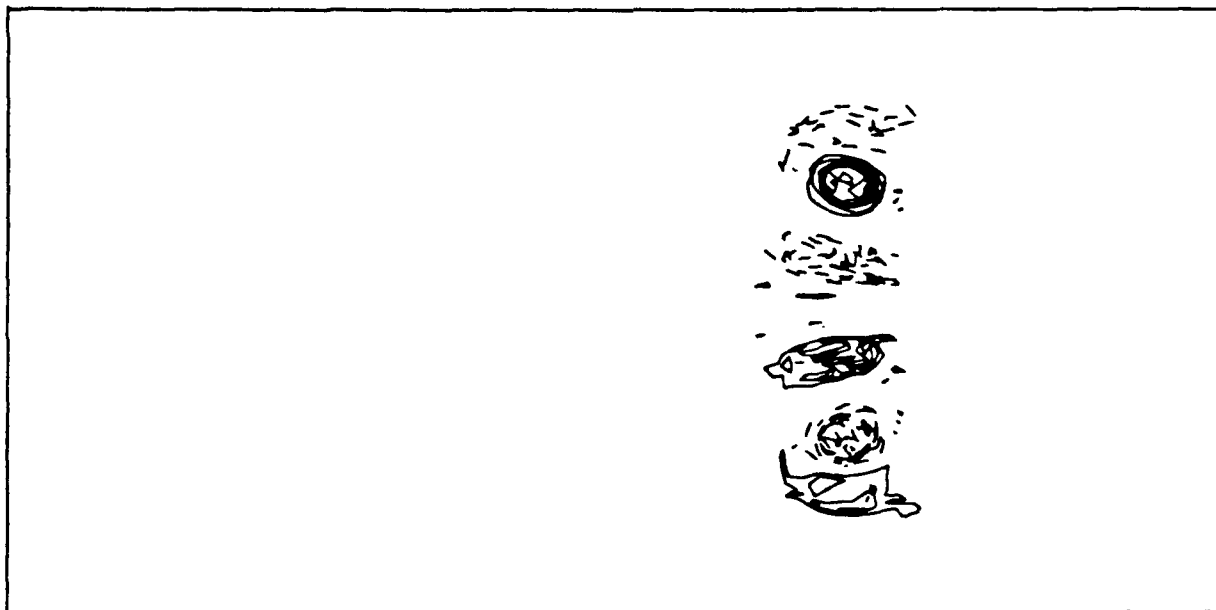
31

(a)

(b)

(c)

(d)

(e)

(f)
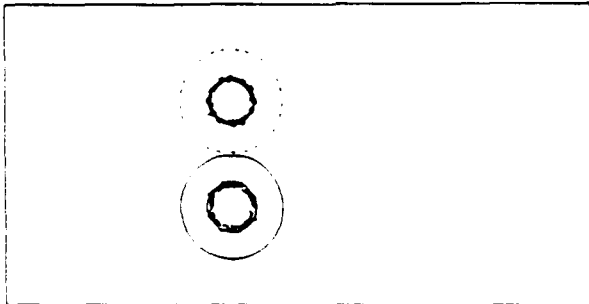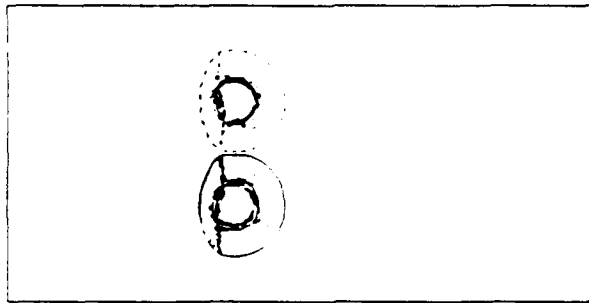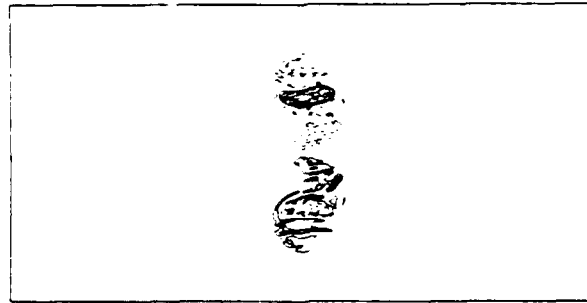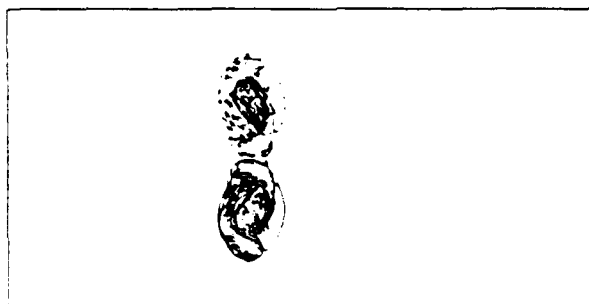
!4. Vorticity contours for strong shock and strong vortex pair at time (a) 0.0145 (b) 0.0435 (c) 0.0725 (d) 0.1015 (e) 0.1595 (f) 0.2175 ms. Contours range from -1.9e5 to -0.1e5 and 0.1e5 to 1.9e5 in intervals of 0.1e5 s^{-1}.
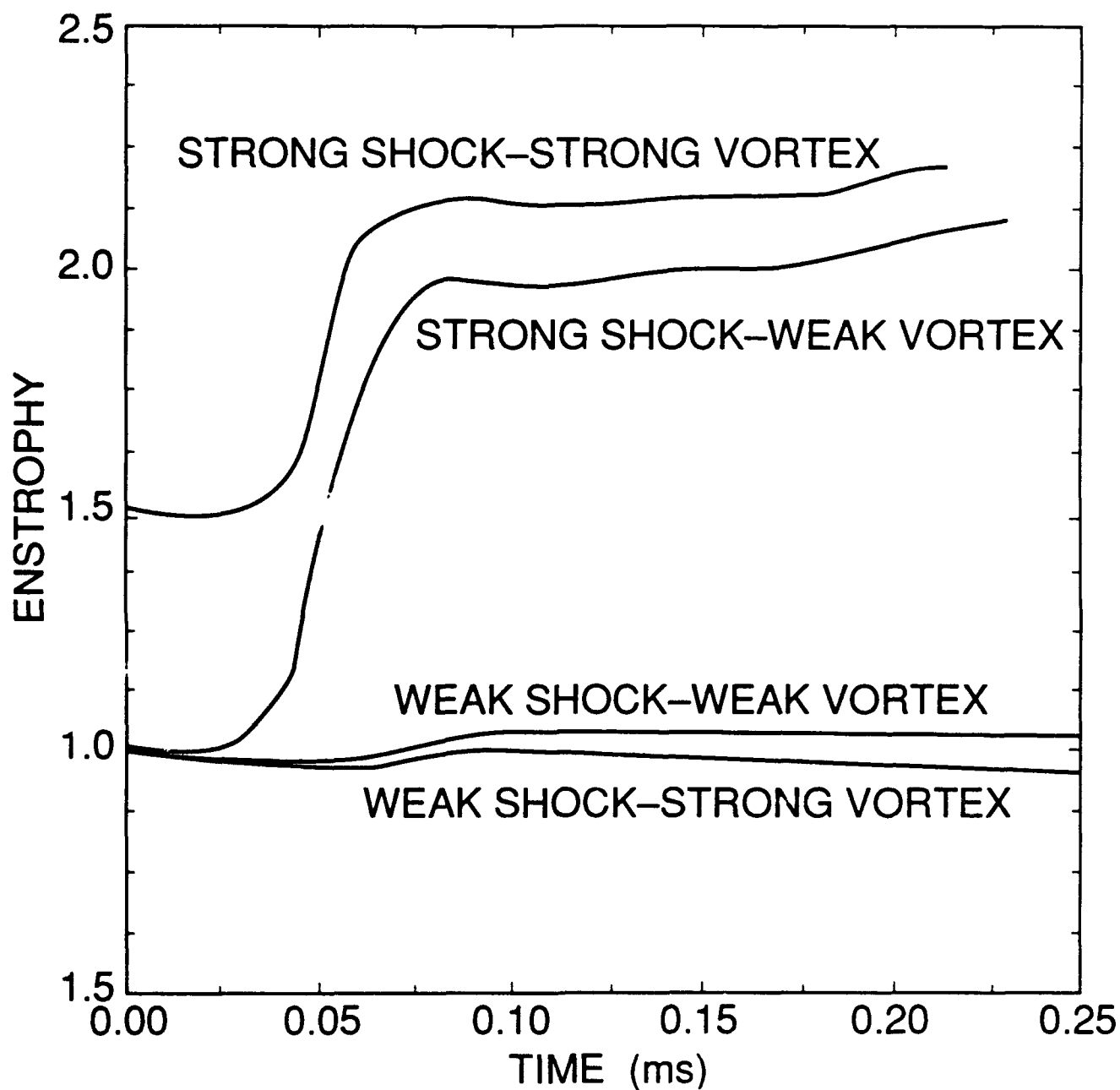
(a)

(b)

15. Steady-state for strong shock and strong vortex pair at time = 0.580 ms (a) pressure difference (b) vorticity.

16. Enstrophy vs time for a) weak vortex and weak shock (b) weak vortex and ₋trong shock (c) strong vortex and weak shock (d) strong vortex strong shock